Materials Research. 2015; 18(6): 1407-1413
DOI: http://dx.doi.org/10.1590/1516-1439.002715

Boron Doped Ultrananocrystalline Diamond Films on Porous Silicon: Morphological, Structural and Electrochemical Characterizations

Lilian Mieko da Silva[a]**, Marta dos Santos[a], Maurício Ribeiro Baldan[a], Antonio Fernando Beloto[a], Neidenêi Gomes Ferreira[a]

[a]Laboratório Associado de Sensores e Materiais, Instituto Nacional de Pesquisas Espaciais – INPE, Jardim da Granja, CEP 12227-010, São José dos Campos, SP, Brazil

Received: September 29, 2015; Revised: October 21, 2015

Boron doped ultrananocrystalline diamond (BDUND) films were grown and characterized on porous silicon (PS) substrates. PS samples were prepared from n-type monocrystalline silicon wafers (100) with 1-20 Ω.cm of resistivity, by electrochemical etching, using HF-acetonitrile solution as electrolyte. BDUND films were grown by Hot Filament Chemical Vapor Deposition using CH_4, H_2 and Ar. The doping process consisted of an additional hydrogen line, passing through a bubbler containing B_2O_3 dissolved in methanol, with boron/carbon ratio of 20000 ppm in solution. Raman spectroscopy and X-Ray diffraction were used to evaluate the quality of the films. Scanning electron microscopy was used for morphological characterization, and confirmed that the films covered the pores without filling them. Electrochemical response and capacitance behavior of the electrodes were explored, by cyclic voltammetry. Samples presented high capacitance, confirming that BDUND/PS electrodes are promising for application as electrochemical capacitors.

Keywords: *boron doped ultrananocrystalline diamond films, porous silicon, electrochemical application, capacitance*

1. Introduction

Porous silicon, which consists of a superficial film with randomly spaced pores, can be obtained by chemical or electrochemical etching of silicon, in hydrofluoric acid solution[1]. The dissolution process is a function of current density, electrolyte concentration, crystal orientation, resistivity and light intensity, which affect pore size and porosity[2]. The conventional method for obtaining PS is through anodizing process under galvanostatic conditions[3]. PS presents extremely rich morphological features and it is a very attractive material for biomedical applications, solar cells, gas sensors, light emitting diodes, among others[4-7]. Furthermore, PS has been used as substrate to thin films growth, including diamond films, in order to increase the number of diamond nucleation sites, improving the films crystalline structure. It presents a large surface area, which makes it an excellent material for obtaining porous electrodes[8,9].

One of the most common methods to grow diamond films is the Chemical Vapor Deposition (CVD) process, which involves gas phase chemical reactions on the substrate surface and results in the deposition of a solid material[10]. Typically, the gas mixture used to obtain diamond films consists of hydrogen and methane. For nanofilms, an inert gas, such as argon or helium, is used in addition to the mixture of hydrogen and methane, in order to promote a continuous transition of grain size from micro to nanocrystalline[11]. Since diamond surface has a high resistivity, doping with boron is performed in order to obtain semiconducting characteristics. Diamond p-type doping has been achieved by boron substitutional process during the film growth[12].

For diamond growth, PS can influence the nucleation, strain and crystal structure of the films grown on its surface. CVD diamond nucleation occurs preferentially at active sites such as surface defects, vertices and atoms edges. The combination of PS morphology control, associated to its pre-treatment, may be mandatory to obtain good quality diamond films[13]. Thus, the nucleation and growth of the diamond film depends on the PS roughness and porosity, besides thermodynamic deposition parameters[14].

The establishment of a doping method of CVD diamond films allowed a wide range of application possibilities of these semiconductor films in different areas of science. One of the applications that aroused most interest was the electrodes manufacture to use in electrochemical applications[12]. Boron doped diamond films grown on porous electrodes have shown excellent electrochemical properties associated with their surface area and dopant concentration[15]. Thus, electrochemical studies have shown that nanocrystalline diamond (NCD)/PS electrodes have high capacitive background current, mainly due to the large surface area, making them excellent electrochemical capacitors[8].

Since NCD/PS has show to be a great material for electrochemical applications, in this work, BDUND films were grown on PS, in order to produce not only a porous material, but a boron doped electrode. PS substrates were characterized by Scanning Electron Microscopy (SEM) and Raman scattering spectroscopy. Morphological and

*e-mail: lilian_mieko@yahoo.com.br

structural characterization of BDUND/PS electrodes were made by SEM, Raman spectroscopy and X-ray diffraction. Electrochemical characterization was performed by cyclic voltammetry.

2. Experimental Procedures

Porous silicon samples were obtained from n-type monocrystalline silicon wafers (100) with 1-20 Ω.cm of resistivity, by electrochemical etching, using HF-acetonitrile solution as electrolyte. The silicon backside was previously covered with indium to promote a good ohmic contact. The electrodes were polarized under current density of 56.5 mA/cm^2 for 120 min while a 50 W dichroic lamp was positioned above the system. After anodization, samples were rinsed in deionized water and dried in nitrogen gas.

BDUND films were grown by Hot Filament Chemical Vapor Deposition (HFCVD) technique using CH_4, H_2 and Ar. Films were deposited on PS substrate after seeding pretreatment, in PDDA polymer solution and KCl colloidal solution containing 4 nm diamond particles[16,17]. The doping process consisted of an additional hydrogen line, passing through a bubbler containing B_2O_3 dissolved in methanol, with boron/carbon ratio of 20000 ppm in solution. There were used five linear tungsten wires with 125 µm of diameter as filaments, placed side by side with a 7 mm distance between them. The applied current was 15 A and the pressure inside the reactor was 30 Torr. One film was grown for 3h, using 18/1.5/80 sccm of H_2/CH_4/Ar. Another one was grown for 4h, using 18.5/1.0/80 sccm of H_2/CH_4/Ar.

PS as well as BDUND/PS morphologies were analyzed by SEM images using a JEOL JSM-5310 microscope system, whereas their structural characterizations were made by micro-Raman scattering spectroscopy using a Renishaw microscope system 2000. In addition, BDUND/PS patterns were obtained by X-ray diffraction using a high resolution Philips difractometer, X'Pert model, with the $CuK_{\alpha 1}$ radiation (λ = 0.154 nm) in grazing incident mode with an incident angle of 1°. The average grain size was estimated by Scherrer equation[18], from the broadening of X-ray <111> peak. In order to confirm the average grain size, Field Emission Gun (FEG)-SEM images were made by a TESCAN MIRA 3 microscope system.

Electrochemical characterizations were made by cyclic voltammetry, which was performed at room temperature, using a potentiostat AUTOLAB – PGSTAT 302. It was used 0.5 mol/L H_2SO_4 as electrolyte at a scan rate of 50 mV/s. A three electrode system was used in this study, consisting of a work electrode (sample), a counter electrode (platinum) and a reference electrode (Ag/AgCl).

3. Results and Discussion

SEM images of PS sample obtained by electrochemical etching are presented in Figure 1, in two different magnifications. As observed in the image, PS shows large pores uniformly distributed over the surface. This morphology provides large surface area, making it ideal for diamond films growth.

Figure 2 shows the Raman spectrum of PS sample. It presents the silicon peak shifted to 518 cm^{-1} from the crystalline silicon peak, 520.5 cm^{-1}, which is typical of porous silicon[19]. The photoluminescence band, centered in approximately 4300 cm^{-1}, is also a PS feature[20].

BDUND films were grown for 3 and 4h on PS substrates. Figure 3 shows SEM images of these samples. Both of them presented good nucleation and films coalescence, with uniform morphology. BDUND films covered the bottom and the top surfaces of the pores, as well as its walls, without filling them, keeping the suitable sample porosity.

It is known that the presence of pores on the Si surface increases the nucleation density of carbonaceous materials. The nucleation density on PS is far higher than that on monocrystalline Si. One possible explanation for this is the fact that PS is almost entirely covered by hydrogen atoms[21]. The atomic hydrogen on PS surface stabilizes the formation of the C-H bond, which is a primary precursor to diamond crystallization, and also attacks the amorphous carbon that blocks the nucleation of diamond. Moreover, PS displays a large number of surface defects, which increases the formation of nuclei for diamond growth[13]. Thus, it was possible to obtain homogeneous diamond films on PS with growth times of 3 and 4h, which is considered a quite fast process for CVD diamond films.

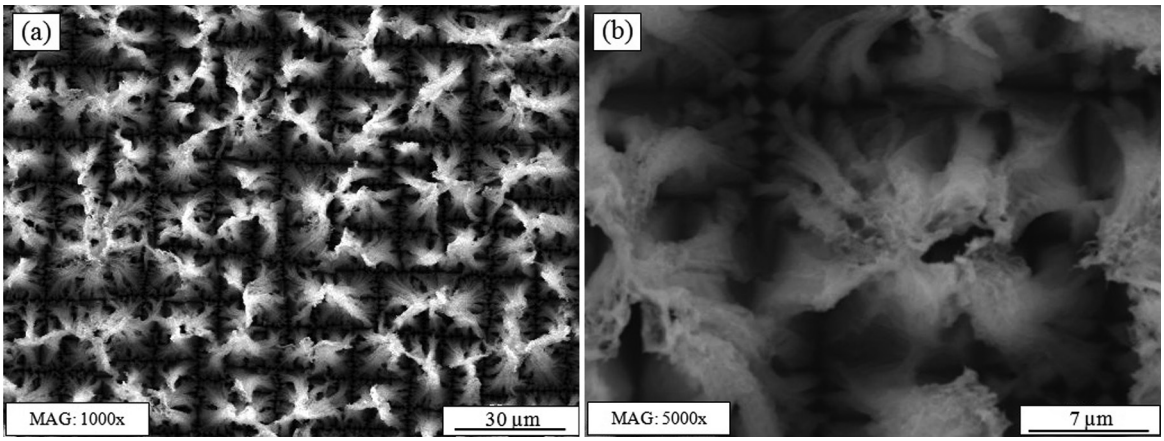

Figure 1. SEM images of porous silicon, in different magnifications (a) 1000x (b) 5000x.

Figure 4 shows Raman spectra of BDUND/PS electrodes grown in 3 and 4h. As can be seen, both spectra showed ultrananocrystalline diamond (UNCD) features, such as, the D band (1345 cm^{-1}), which arises due to sp^2 disorder, and the G band (1550 cm^{-1}), related to sp^2 amorphous carbon. The band around 2670 cm^{-1} is called G'. This band and other remaining peaks of lesser intensity in the high frequencies region can be assigned to overtones (frequency higher than the fundamental frequency), and combinations of modes, i.e., processes that involve two or more phonons, the fundamental vibrations modes of small cross section or double resonance processes[22,23].

Furthermore, the spectra do not present a diamond one-phonon line around 1332 cm^{-1}, as it is verified for single crystal diamond, because this peak was hidden by the strong scattering of sp^2 carbon components in these films. Besides, the broadening of this peak, related to the D band present at 1345 cm^{-1}, overlapped the diamond peak. This behavior is usually noted in NCD using Raman excitation in the visible region[24].

For NCD and UNCD films, the shoulders at 1150 cm^{-1} and 1490 cm^{-1} have been ascribed to the transpolyacetylene (TPA) segments presence at the grain boundaries[25]. Nonetheless, in more recent paper, authors did not agree with this analysis. They used Raman spectroscopy with different wavelengths and discussed the TPA decomposition at temperature lower than that for the film growth. In conclusion, the peak at 1150 cm^{-1} was attributed to the deformation mode of the CH_x bond[26].

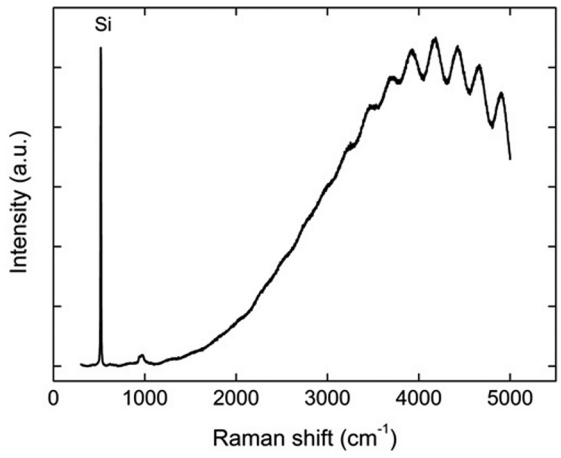

Figure 2. Raman spectrum of porous silicon.

The X-ray diffraction patterns of the BDUND/PS electrodes are presented in Figure 5. Although films present lower thickness, it is possible to observe the peaks at 43.9°, 75.3° and 91.5° corresponding to the (111), (220) and (311) diamond diffraction peaks, which confirm the presence of crystalline diamond[27]. In addition, two silicon peaks at 47° (220) and 56° (331) can be seen. Despite the measures have been made with grazing angle of 1.0°, it was detected the Si presence in both samples, since the films are very thin and the X-ray penetration depth is very high in carbonaceous materials.

It is also possible to observe peaks at 57° and 88°, probably associated with silicon carbide (SiC). The SiC layer always exists between the diamond and the Si substrate[28]. In the case of PS substrate, it is easily carbonized during growth due to its porous structure. Thus, the PS layer is almost completely carbonized in a SiC porous layer, resulting in its respective diffraction peaks in the patterns[29]. This SiC formation, which usually occurs on the edge and top of the pores, can be related to high adhesion between diamond and PS[14].

The average grain size was calculated by Scherrer equation[18], from the <111> peak. The obtained value was around 5 nm. This value indicates that the films might be ultrananocrystalline, which are characterized by presenting grain size range from 2 to 10 nm[24]. FEG-SEM images were made to confirm this assumption and are shown in Figure 6. The films exhibit non-columnar growth, which reflects on a surface formed by agglomerates of grains, characteristic of UNCD films[24]. Figure 6a shows that the agglomerates sizes are around 240 nm. In Figure 6b, the larger grains inside the agglomerate present size around 11 nm. Smaller grains could not be measured due to equipment limitations (616 kx) in a good focal view. However, these images evidenced the films ultrananocrystalline morphologies.

Electrochemical characterization was made by cyclic voltammetry. It was possible to obtain the work potential window of BDUND/PS electrodes, grown in 3 and 4h,

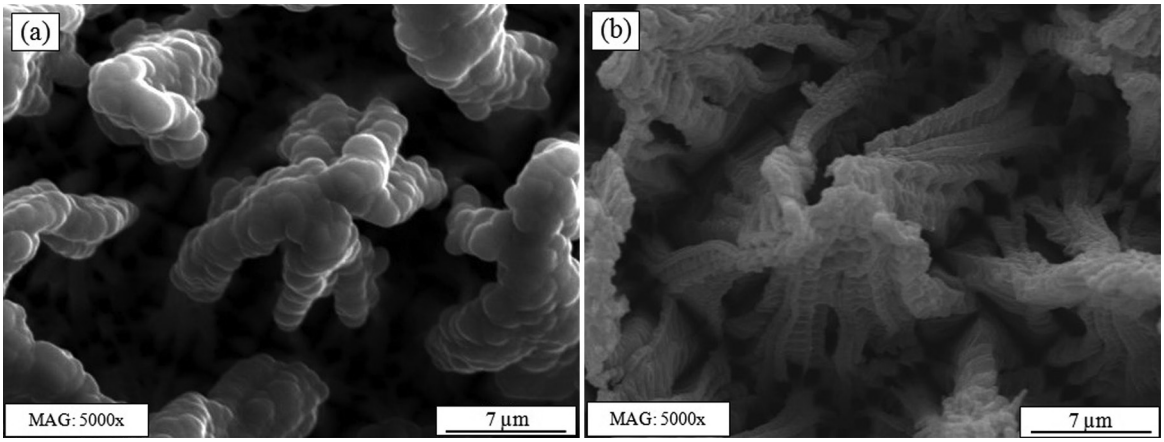

Figure 3. SEM images of BDUND grown on PS for (a) 3h and (b) 4h.

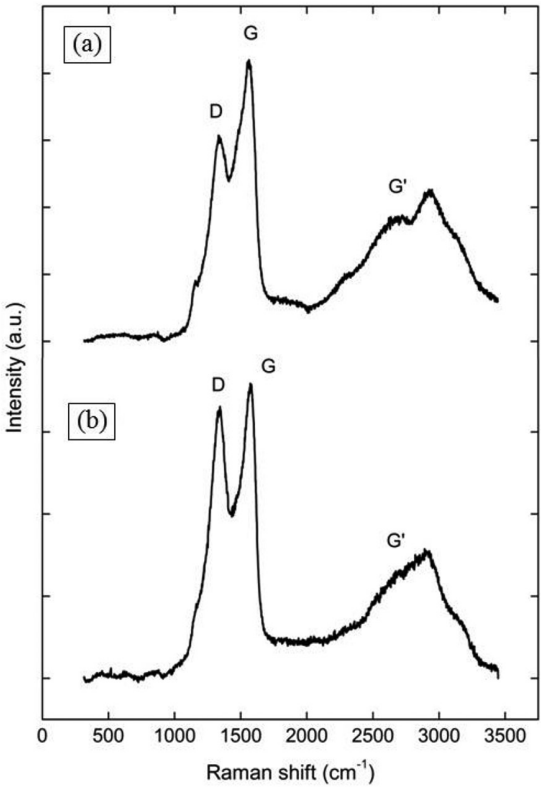

Figure 4. Raman spectra of BDUND grown on PS for (a) 3h and (b) 4h.

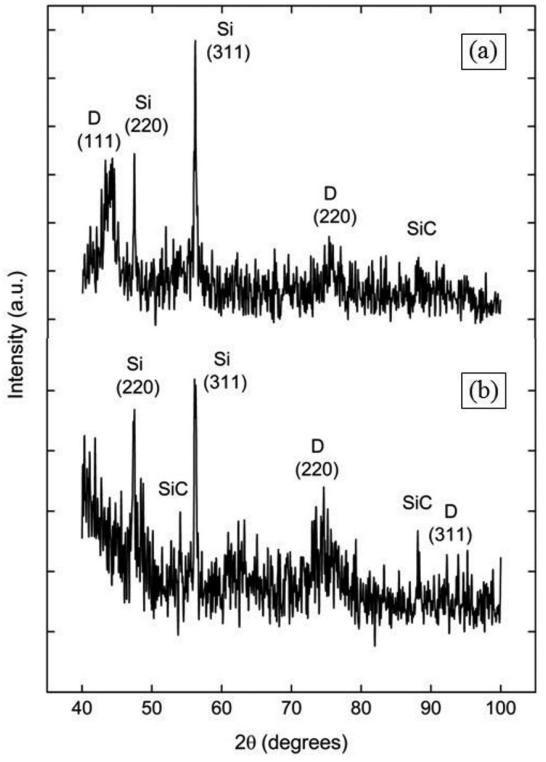

Figure 5. X-ray diffraction spectra of BDUND grown on PS for (a) 3h and (b) 4h.

using a BDUND/Si work potential window as comparison parameter, as shown in Figure 7a. The BDUND/Si electrode, used for comparison, also presents doping of 20000 ppm B/C in solution. The current densities were obtained from the geometric area. Figure 7b shows a zoom view of the voltammograms in the central region, in a small potential range, to compare the current background and to highlight the capacitive effect of BDUND/PS.

As expected for porous electrodes, it is possible to observe the large capacitive effect in black and red curves, which occurs due to the large active area of the BDUND/PS electrodes, as shown in SEM images. These electrodes also showed resistive behavior, which was corrected in the figure by IR compensation. This compensation was performed in the potential region around zero (0.0 V × Ag/AgCl), where it is possible to separate the contribution of the electrode resistance in the current value.

It is also possible to observe that the hydrogen evolution process for BDUND/Si electrode starts at much less negative potential, indicating that this electrode is more conductive. The anodic and cathodic small shoulders appearing in BDUND/PS samples, indicated by (I) and (II) in Figure 7a, represent redox transitions of containing oxygen functional groups, due to the large amount of sp^2 bonds present in NCD films[30].

Considering the anodic current densities for the three electrodes in the zero region potential, it is possible to obtain values of the order of 4.6×10^{-6}; 2.4×10^{-4} and 1.8×10^{-4} for the BDUND/Si, BDUND/PS-3h and BDUND/PS-4h electrodes, respectively. These results show a capacitive current of two orders of magnitude higher for samples grown on PS. From these results, it is possible to obtain the electrodes capacitance. The capacitance (C) is the proportionality coefficient between the capacitive current (I) and the scanning speed (v), that is C = I/v. Figure 8 presents the capacitance results for the three electrodes.

The capacitance values increased with the potential, as expected, especially for the films grown on PS. In 0.8 V × Ag/AgCl, these values are around 300, 6500 and 5500 $\mu F.cm^{-2}$ for the BDUND/Si, BDUND/PS-3h and BDUND/PS-4h electrodes, respectively, considering their geometric areas. Therefore, 3h electrode shows a capacitance value more than 20 times higher than that of BDUND/Si sample.

It is important to note that although the capacitance of the 4h film is higher than that of BDUND/Si, the capacitance tended to decrease when increasing growth time. This fact may be associated to a greater covering of the pores with higher growth time, showing that this is also a limiting factor for electrochemical applications where the capacitive effect should be a dominant factor. In this case, the challenge is to obtain a BDUND layer over PS that promotes a uniform and homogeneous film, covering the walls and the bottom of the pores, but maintaining the porous morphology.

Results are consistent with those found by Ferreira and coworkers[8], in which NCD/PS electrodes showed capacitance values in the range of 230-990 $\mu F.cm^{-2}$ in × 1.0 V × Ag/AgCl. This corresponds to about a 25 times increase, compared

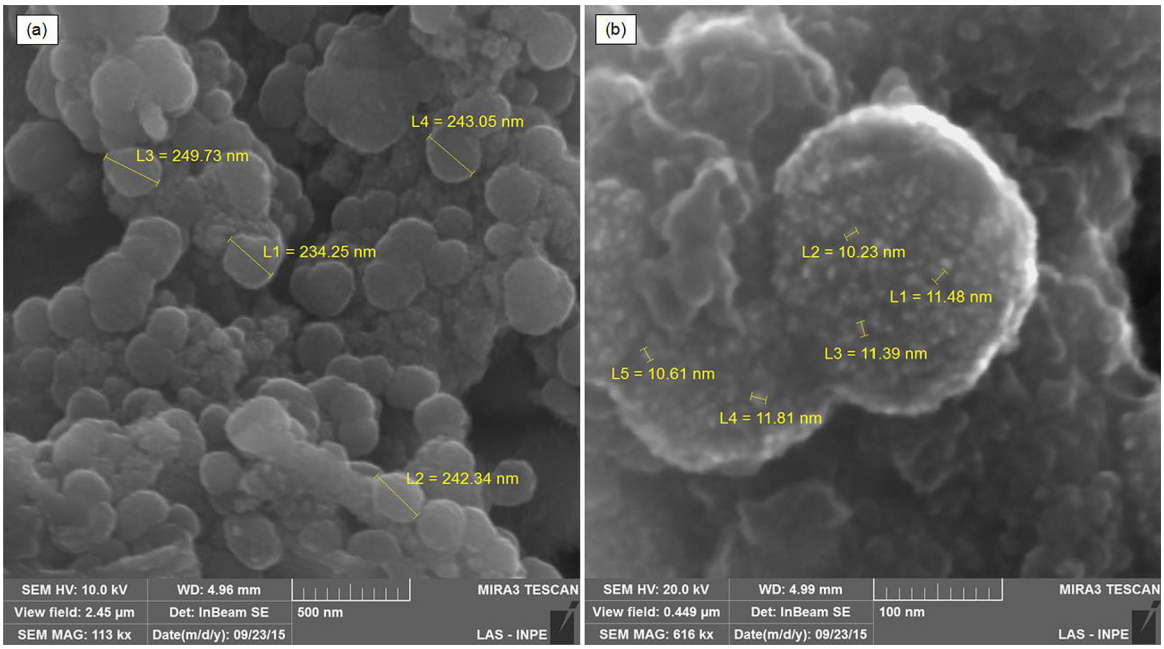

Figure 6. FEG-SEM images of BDUND/PS, in different magnifications (a) 113000x, showing grains agglomerates (b) 616000x, showing grain sizes.

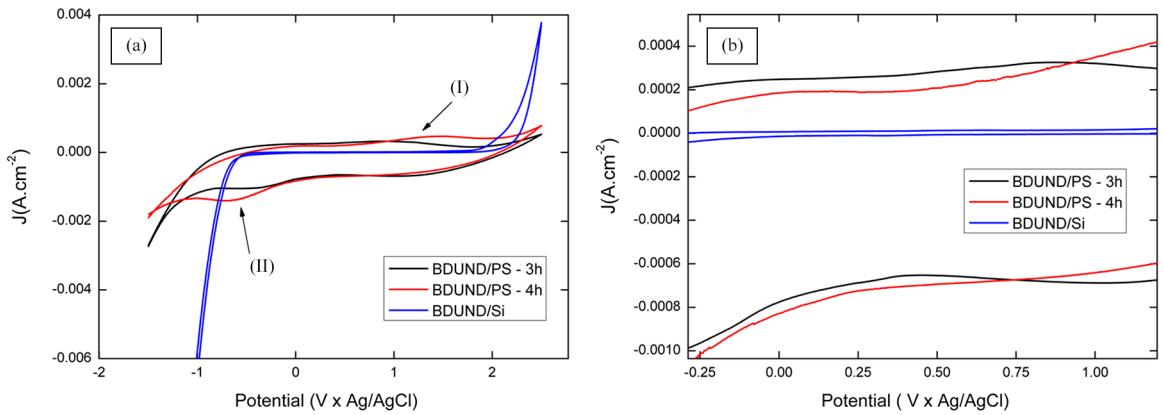

Figure 7. (a) Work potential windows of BDUND/PS grown for 3h and 4h, and of a BDUND/Si sample, (b) Zoom view of the work potential windows.

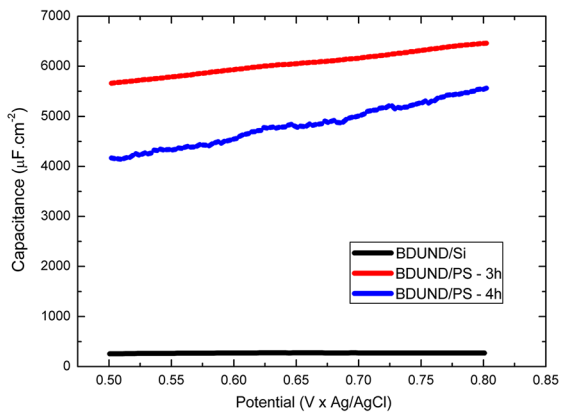

Figure 8. Capacitance values for the three electrodes.

to boron doped microcrystalline diamond electrodes. The electrodes capacitance curve, in the studied potential range, presented a similar behavior to that observed in Figure 8, in which the capacitance increases as a function of the potential.

These results also showed good agreement with the values found by Honda and coworkers[31]. For their nanohoneycomb diamond electrode, the capacitance value at 1.0 V × Ag/AgCl was 190 µF.cm^{-2}, 15 times greater than that for their diamond electrode. They attributed the high capacitance values to the formation of highly ordered porous structure, as well as, to the surface oxidation. The BDUND/PS electrodes obtained in this study showed a capacitance value about 30 times greater than that of nanohoneycomb diamond obtained by Honda et al.[31].

4. Conclusions

BDUND films were successfully grown and characterized on PS substrate. SEM images confirmed that BDUND films covered the whole PS surface, including the pores bottom and their internal walls, maintaining the substrate porous structure and providing greater surface area, which is ideal for diamond films growth. Structural characterization confirmed the diamond presence. Raman spectra presented the D and G bands, features of UNCD films. In X-ray diffraction patterns, it was possible to observe the peaks corresponding to the (111), (220) and (311) diamond diffraction peaks. FEG-SEM images showed the ultrananocrystalline film morphology. Electrochemical characterization showed high capacitance values for BDUND/PS samples, as expected for porous electrodes, confirming that BDUND/PS electrodes are promising for electrochemical applications.

Acknowledgements

The authors would like to thank CAPES and FAPESP for financial support and M. L. B. Matos for SEM images.

References

1. Cho B, Jin S, Lee BY, Hwang M, Kim HC and Sohn H. Investigation of photoluminescence efficiency of n-type porous silicon by controlling of etching times and applied current densities. *Microelectronic Engineering*. 2012; 89:92-96. http://dx.doi.org/10.1016/j.mee.2011.03.145.
2. Kang CG, Kang MS and Yang JH. Comparison of nano-porous silicon prepared by photoelectrochemical etching in HF-ethanol and HF-acetonitrile solutions. *Journal of the Korean Physical Society*. 2003; 42:S693-S697.
3. Miranda CRB, Baldan MR, Beloto AF and Ferreira NG. Morphological and optical characteristics of porous silicon produced by anodization process in HF-acetonitrile and HF-ethanol solutions. *Journal of the Brazilian Chemical Society*. 2008; 19(4):769-774. http://dx.doi.org/10.1590/S0103-50532008000400022.
4. Santos HA. *Porous silicon for biomedical applications*. Cambridge: Woodhead Publishing; 2014.
5. Milenkovic N, Drießen M, Gust E, Janz S and Reber S. Reorganization of porous silicon: effect on epitaxial layer quality and detachement. *Energy Procedia*. 2014; 55:552-558. http://dx.doi.org/10.1016/j.egypro.2014.08.023.
6. Park SH, Kim YY and Lee KW. Sensitivity improvement of free-standing porous silicon rugate filters for isopropanol vapor detection by applying lateral pressure differences. *Sensors and Actuators B, Chemical*. 2013; 176:437-442. http://dx.doi.org/10.1016/j.snb.2012.09.045.
7. Xie Z and Blackwood DJ. White electroluminescence from ITO/porous silicon junctions. *Journal of Luminescence*. 2013; 143:67-70. http://dx.doi.org/10.1016/j.jlumin.2012.09.012.
8. Ferreira NG, Azevedo AF, Beloto AF, Amaral M, Almeida FA, Oliveira FJ, et al. Nanodiamond films growth on porous silicon substrates for electrochemical applications. *Diamond and Related Materials*. 2005; 14(3-7):441-445. http://dx.doi.org/10.1016/j.diamond.2005.01.007.
9. Sánchez de la Morena S, Recio-Sánchez G, Torres-Costa V and Martín-Palma RJ. Hybrid gold/porous silicon thin films for plasmonic solar cells. *Scripta Materialia*. 2014; 74:33-37. http://dx.doi.org/10.1016/j.scriptamat.2013.06.015.
10. Angus JC. Diamond synthesis by chemical vapor deposition: the early years. *Diamond and Related Materials*. 2014; 49:77-86. http://dx.doi.org/10.1016/j.diamond.2014.08.004.
11. Azevedo AF and Ferreira NG. Filmes de nanodiamantes para aplicações em sistemas eletroquímicos e tecnologia aeroespacial. *Quimica Nova*. 2006; 29(1):129-136. http://dx.doi.org/10.1590/S0100-40422006000100023.
12. Barros RCM, Ribeiro MC, An-Sumodjo PT, Julião MSS, Serrano SHP and Ferreira NG. Filmes de diamante CVD dopado com boro, parte I - histórico, produção e caracterização. *Quimica Nova*. 2005; 28(2):317-325. http://dx.doi.org/10.1590/S0100-40422005000200024.
13. Raiko V, Spitzl R, Engemann J, Borisenko V and Bondarenko V. MPCVD diamond deposition on porous silicon pretreated with the bias method. *Diamond and Related Materials*. 1996; 5(10):1063-1069. http://dx.doi.org/10.1016/0925-9635(96)00514-6.
14. Baranauskas V, Li BB, Peterlevitz AC, Tosin MC and Durrant SF. Structure and properties of diamond films deposited on porous silicon. *Thin Solid Films*. 1999; 355-356:233-238. http://dx.doi.org/10.1016/S0040-6090(99)00488-5.
15. Ferreira NG, Mendonça LL, Trava-Airoldi VJ and Rosolen JM. Electrochemical intercalation of lithium into boron-doped CVD diamond electrodes grown on carbon fiber cloths. *Diamond and Related Materials*. 2003; 12(3-7):596-600. http://dx.doi.org/10.1016/S0925-9635(02)00273-X.
16. Liu X, Yu T, Wei Q, Yu Z and Xu X. Enhanced diamond nucleation on copper substrates by employing an electrostatic self-assembly seeding process with modified nanodiamond particles. *Colloids and Surfaces A, Physicochemical and Engineering Aspects*. 2012; 412:82-89. http://dx.doi.org/10.1016/j.colsurfa.2012.07.020.
17. Campos RA, Trava-Airoldi VJ, Bagnato OR, Moro JR and Corat EJ. Development of nanocrystalline diamond windows for application in synchrotron beamlines. *Vacuum*. 2013; 89:21-25. http://dx.doi.org/10.1016/j.vacuum.2012.09.007.
18. Barbosa DC, Barreto PRP, Trava-Airoldi VJ and Corat EJ. Growth and characterization of diamond micro and nano crystals obtained using different methane concentration in argon-rich gas mixture. *Diamond and Related Materials*. 2010; 19(7-9):768-771. http://dx.doi.org/10.1016/j.diamond.2010.01.040.
19. Cho CH, Seo YS, Na H and Kim Y. Size effects in Raman scattering of porous silicon. *Journal of the Korean Physical Society*. 1998; 33(3):292-296.
20. Kumar P. Effect of silicon crystal size on photoluminescence appearance in porous silicon. *ISRN Nanotechnology*. 2011; 2011:1-6. http://dx.doi.org/10.5402/2011/163168.
21. Van der Veen JF and Van Hove MA. *The Structure of Surface II*. Berlin: Springer-Verlag; 1988.
22. Chu PK and Li L. Characterization of amorphous and nanocrystalline carbon films. *Materials Chemistry and Physics*. 2006; 96(2-3):253-277. http://dx.doi.org/10.1016/j.matchemphys.2005.07.048.
23. Ferrari AC and Robertson J. Interpretation of Raman spectra of disordered and amorphous carbon. *Physical Review B: Condensed Matter and Materials Physics*. 2000; 61(20):14095-14107. http://dx.doi.org/10.1103/PhysRevB.61.14095.
24. Williams OA, Daenen M, D'Haen J, Haenen K, Maes J, Moshchalkov VV, et al. Comparison of the growth and properties of ultrananocrystalline diamond and nanocrystalline diamond.

Diamond and Related Materials. 2006; 15(4-8):654-658. http://dx.doi.org/10.1016/j.diamond.2005.12.009.

25. Ferrari AC and Robertson J. Raman spectroscopy of amorphous, nanostructured, diamond-like carbon, and nanodiamond. *Philosophical Transactions A, Mathematical, Physical, and Engineering Sciences*. 2004; 362(1824):2477-2512. http://dx.doi.org/10.1098/rsta.2004.1452. PMid:15482988.
26. Mortet V, Zhang L, Eckert M, D'Haen J, Soltani A, Moreau M, et al. Grain size tuning of nanocrystalline chemical vapor deposited diamond by continuous electrical bias growth: experimental and theoretical study. *Physica Status Solidi A, Applications and Materials Science*. 2012; 209(9):1675-1682. http://dx.doi.org/10.1002/pssa.201200581.
27. Azevedo AF, Ramos SC, Baldan MR and Ferreira NG. Graphitization effects of CH_4 addition on NCD growth by first and second Raman spectra and by X-ray diffraction measurements. *Diamond and Related Materials*. 2008; 17(7-10):1137-1142.
28. Kobayashi K, Karasawa S, Watanabe T and Togashi F. Growth of diamond thin films on silicon and TEM observation of the interface. *Journal of Crystal Growth*. 1990; 99(1-4):1211-1214. http://dx.doi.org/10.1016/S0022-0248(08)80110-8.
29. Liu Z, Zong BQ and Lin Z. Diamond growth on porous silicon by hot-filament chemical vapor deposition. *Thin Solid Films*. 1995; 254(1-2):3-6. http://dx.doi.org/10.1016/0040-6090(95)80010-7.
30. Huang CW, Wu YT, Hu CC and Li YY. Textural and electrochemical characterization of porous carbon nanofibers as electrodes for supercapacitors. *Journal of Power Sources*. 2007; 172(1):460-467. http://dx.doi.org/10.1016/j.jpowsour.2007.07.009.
31. Honda K, Rao TN, Tryk DA, Fujishima A, Watanabe M, Yasui K, et al. Electrochemical characterization of the nanoporous honeycomb diamond electrode as an electrical double-layer capacitor. *Journal of the Electrochemical Society*. 2000; 147(2):659-664. http://dx.doi.org/10.1149/1.1393249.